Supporting Information

Coupling Calcination–Sulfidation Strategy to Fabricate Hydrophilic Bimetallic Transition Nanozyme for Boosting Antibacterial Efficiency

Tianshuo Wang,[†] Yuhang Lin,[†] Lianxi Pu,[†] Yinmin Min, [†] Min Zhang, [†] Deping Wang[†]

Lijun Ding[‡]*, Kun Wang[†]*

[†]*School of Chemistry and Chemical Engineering, Jiangsu University, Zhenjiang 212013, PR China.*

E-mail: *wangkun@ujs.edu.cn (K. Wang)*

[‡]*School of Agricultural Engineering, Jiangsu University, Zhenjiang 212013, PR China.*

E-mail: *ljding@ujs.edu.cn (L. Ding), wangkun@ujs.edu.cn (K. Wang)*

Content

1. Reagents and Apparatus

1.1 Reagents

Hydroquinone (HQ), 5,5-Dimethyl-1-Pyrroline-N-Oxide (DMPO), Benzoquinone (PBQ), terephthalic acid (TA), L-histidine (L-His), etc. were purchased from Leyan Reagent Company. Thiourea (TH), and ascorbic acid (AA) were purchased from Shanghai Yuanye Bio-Technology Co., Ltd. Potassium ferrocyanide ($[K_3Fe(CN)_6]$) and cobalt chloride dihydrate(II) ($CoCl_2 \cdot 6H_2O$) were purchased from Sigma Aldrich. Polyvinylpyrrolidone (PVP) and trisodium citrate ($C_6H_5Na_3O_7$) were purchased from Jiangsu Kaiwei Chemical Co., Ltd. 3,3',5,5'-Tetramethylbenzidine (TMB), Sodium sulfide (Na_2S) and phosphate buffered saline (PBS) were purchased from Shanghai Macklin Biochemical Co., Ltd. All chemicals were used as received without any further purification.

1.2 Apparatus

The surface morphology of the synthesized materials was analyzed using a Scanning Electron Microscope (SEM, Apreo S HiVac, Thermo Fisher Scientific, USA). To characterize the crystal structure, functional groups, and elemental composition/valence states of the materials, X-ray Diffraction (XRD, Bruker D8 Advance, Germany), Fourier Transform Infrared Spectroscopy (FT-IR, Nicolet iS50, Thermo Fisher Scientific, USA), and X-ray Photoelectron Spectroscopy (XPS, ESCALAB QXi, Thermo Fisher Scientific, USA) were employed, respectively. Electron Spin Resonance (ESR, Bruker EMX Plus, Germany) and Inductively Coupled Plasma Mass Spectrometry (ICP-MS, ICP-MS 2030LF, Shimadzu, Japan) were used to verify the presence of specific defects and elemental leaching. The catalytic performance was assessed using an X-ray Fluorescence Spectrometer (XRF, Panalytical Axios, Netherlands) and an Ultraviolet-Visible Spectrophotometer (UV-Vis, Shimadzu UV2600, Japan). Specific surface area and porosity were determined by Nitrogen Physisorption measurements (BET, TriStar II 3020, Micromeritics, USA). Thermal stability was evaluated via Thermogravimetric Analysis (TGA, STA 449C,

Netzsch, Germany). Raman spectra were recorded on a Raman Spectrometer (RS, Thermo Fisher, USA). Temperature-Programmed Desorption (TPD) experiments were conducted on a BelCata II apparatus (Bel Japan, Japan). A Constant Temperature Water Bath Shaker (CHA C, China) was used for solution mixing and reaction incubation. All instruments were used according to the manufacturers' standard protocols.

2. Experimental section

2.1 Preparation of CoFePBA

Based on the literature protocol,[1] CoFePBA was prepared with slight modifications. 0.066 g of potassium ferricyanide [$K_3Fe(CN)_6$] was dissolved in 20 mL of deionized water, while 0.1428 g of cobalt chloride hexahydrate ($CoCl_2 \cdot 6H_2O$), 0.25 g of trisodium citrate ($C_6H_5Na_3O_7$), and 0.3 g of polyvinylpyrrolidone (PVP) were dissolved in another 30 mL of deionized water. The two solutions were mixed and stirred for 24 h. The precipitate was collected by centrifugation at 12,000 g for 5 min, then washed three times with deionized water and ethanol respectively. Finally, the product was dried in an oven at 60 °C for 24 h to obtain CoFePBA.

2.2 Preparation of CoFePBA-N_2-300

100 mg of CoFePBA was placed in a ceramic boat and transferred into a tube furnace. Under a nitrogen atmosphere, the temperature was raised from room temperature to 300 °C at a heating rate of 5 °C/min and maintained for 3 h. After cooling to room temperature, the product was ground and stored in a sealed container, yielding CoFePBA-N_2-300.

2.3 Preparation of CoS_2/FeS_2@NCF

20 mg of CoFePBA-N_2-300 was dispersed in 20 mL of ethanol via ultrasonication. Separately, 80 mg of Na_2S was dispersed in 10 mL of deionized water. The two solutions were then mixed and transferred into a 50 mL Teflon-lined stainless-steel autoclave. The mixture was heated to 180 °C and maintained at this temperature for 2 h. After natural cooling, the product was washed multiple times with deionized water and ethanol, dried overnight under vacuum at 60 °C, ground, and stored in a sealed container, yielding CoS_2/FeS_2@NCF.

2.4 POD-like activity test

The POD-like activity of the synthesized CoS_2/FeS_2@NCF was investigated via the TMB oxidation colorimetric method. A mixture containing 25 μL of CoS_2/FeS_2@NCF aqueous dispersion (0.40 mg/mL), 775 μL of PBS (pH = 4.0, 200

mM), and 100 μL of H_2O_2 (10 mM) was prepared. Subsequently, 100 μL of TMB (5 mM) was added to this mixture. The color change of the reaction solution was then observed, and its absorbance peak at 652 nm was recorded using a UV-vis spectrophotometer.

2.5 Antibacterial activity test

The plate counting method was used to test the antibacterial effects of different concentrations of H_2O_2 and the antibacterial activity of nanozymes.[2] First, solid and liquid media were prepared for bacterial incubation and autoclaved at high pressure for 1 h. The primary bacteria were transferred to liquid media and incubated overnight at 37 °C with constant temperature, after which the bacterial dispersion was centrifugally washed three times with PBS buffer solution. The blank group contained a bacterial solution at a concentration of 105 CFU/mL, while the experimental groups were prepared by mixing 105 CFU/mL bacterial solutions with catalyst solutions of different concentrations. For testing the antibacterial effects of different H_2O_2 concentrations, the added H_2O_2 concentrations were 0.05, 0.1, 0.5, 1, 2, 3, 5 and 10 mmol/L. For testing the antibacterial activity of nanozymes, combinations of 100 μg/mL nanozymes with 1 mmol/L H_2O_2, 200 μg/mL nanozymes with 2 mmol/L H_2O_2, and 300 μg/mL nanozymes with 3 mmol/L H_2O_2 were added, respectively. For each group, 200 μL of the mixed solution was evenly spread on the surface of solid media and incubated at 37 °C for 12 h. The antibacterial effects of the compounds were quantitatively analyzed by counting the number of bacterial colonies formed on the solid media surface.

2.6 SEM observation of bacterial morphology experiment

The in situ fixation method was used to obtain bacterial sections.[3] After incubating the primary bacteria at 37 °C for 24 h, they were centrifugally washed three times with deionized water to obtain a bacterial suspension. Then, the compound solution at the corresponding concentration was added to the bacterial suspension at a concentration of 109 CFU/mL and fixed with 2.5% glutaraldehyde solution for 10 h. Next, the mixed solution was dehydrated by washing and centrifuging with ethanol aqueous solutions at concentrations of 20%, 40%, 60%, 80%, and 100% in sequence. Finally, the sample

was dropped onto a conductive adhesive, subjected to gold sputtering treatment, and the morphological changes of bacteria were observed by scanning electron microscopy (SEM).

3. Results and Discussion

3.1. Characterization of CoS_2/FeS_2@NCF

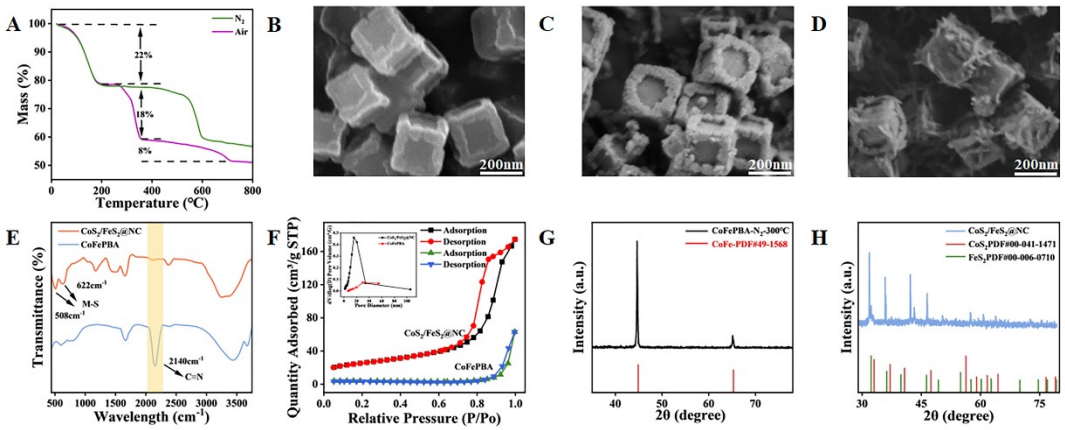

Fig. S1 (A) TGA curves of CoFePBA in N_2 and air; SEM images of (B) CoFePBA, (C) CoFePBA-N_2-300 and (D) CoS_2/FeS_2@NCF (E) FT-IR spectra of CoFePBA and CoS_2/FeS_2@NCF; (F) Nitrogen adsorption-desorption curves and corresponding pore size distribution of CoFePBA and CoS_2/FeS_2@NCF; XRD pattern of (G) CoFePBA-N_2-300 and (H) CoS_2/FeS_2@NCF

Raman spectroscopy was further employed to investigate the structure of the nitrogen-doped carbon framework in CoFePBA and CoS_2/FeS_2@NCF nanocube (Fig. S2A). The Raman spectrum of CoFePBA showed no carbon framework features. In contrast, the spectrum of CoS_2/FeS_2@NCF exhibited two prominent peaks at 1353 cm^{-1} and 1590 cm^{-1}, corresponding to the D-band (disordered carbon) and G-band (graphitic carbon), respectively.[4] The calculated I_D/I_G ratio of 1.08 indicates a predominantly amorphous nature due to structural defects induced by calcination, while simultaneously suggesting the highly conductive properties of the carbon framework.[5]

X-ray photoelectron spectroscopy (XPS) measurements were performed to analyze the chemical states of the CoS_2/FeS_2@NCF nanocube. Survey and high-resolution spectra of the C 1s, N 1s, S 2p, Co 2p, and Fe 2p regions are presented. The formation of the nitrogen-doped carbon framework was confirmed by the C 1s and N 1s spectra (Fig. S2B-C). Peaks in the C 1s spectrum were deconvoluted at 284.6 eV (C-C), 285.9 eV (C-N), and 288.3 eV (C-S).[6] Compared to CoFePBA, the C-C peak

position remained unchanged. The newly emerged C-S peak confirms sulfur doping into the metal-carbon matrix. The C-N peak shifted to higher binding energy, which may be attributed to the thermally induced transformation of C-N bonds into more polar C=N bonds and/or the electron-withdrawing inductive effect of neighboring sulfur atoms, depleting electron density from the carbon in C-N bonds and thus increasing its binding energy. Peaks in the N 1s spectrum were assigned to pyridinic N (399.6 eV) and pyrrolic N (400.8 eV).[7] Pyridinic N can modulate the electronic structure of carbon and effectively enhance the immobilization within CoS_2/FeS_2@NCF.[8] After calcination-sulfidation, the pyrrolic N peak shifted to higher binding energy, while the pyridinic N peak shifted to lower binding energy. This is primarily due to altered electronic environments: sulfur coordination reduces the electron density around pyrrolic N (increasing binding energy), whereas metal bonding enriches electron density around pyridinic N (decreasing binding energy), reflecting differential regulation of the local electronic structure. This confirms the successful preparation of a PBA-derived framework rich in carbon and nitrogen atoms.[9] The S 2p spectrum (Fig. S2D) was deconvoluted into four main peaks at 162.3 eV, 162.7 eV, 163.6 eV, and 164.4 eV, corresponding to S^{2-} and S_2^{2-} species.[10] An additional broad peak observed at 168.4 eV may arise from partial surface oxidation of sulfur.[6] The peak positions for Co and Fe showed no shift compared to the CoFePBA precursor. Peaks at 781.3 eV, 797.0 eV, 782.5 eV, and 798.1 eV were assigned to Co^{3+} $2p^{3/2}$, Co^{3+} $2p^{1/2}$, Co^{2+} $2p^{3/2}$, and Co^{2+} $2p^{1/2}$, respectively (Fig. S2E)[11,12]. In the Fe 2p spectrum (Fig. S2F), two distinct peaks related to Fe $2p^{3/2}$ and Fe $2p^{1/2}$ were observed at 707.4 eV and 720.1 eV, respectively.[13] Collectively, these analyses provide comprehensive evidence for the successful formation of the nitrogen-doped carbon framework and sulfidation of the material.

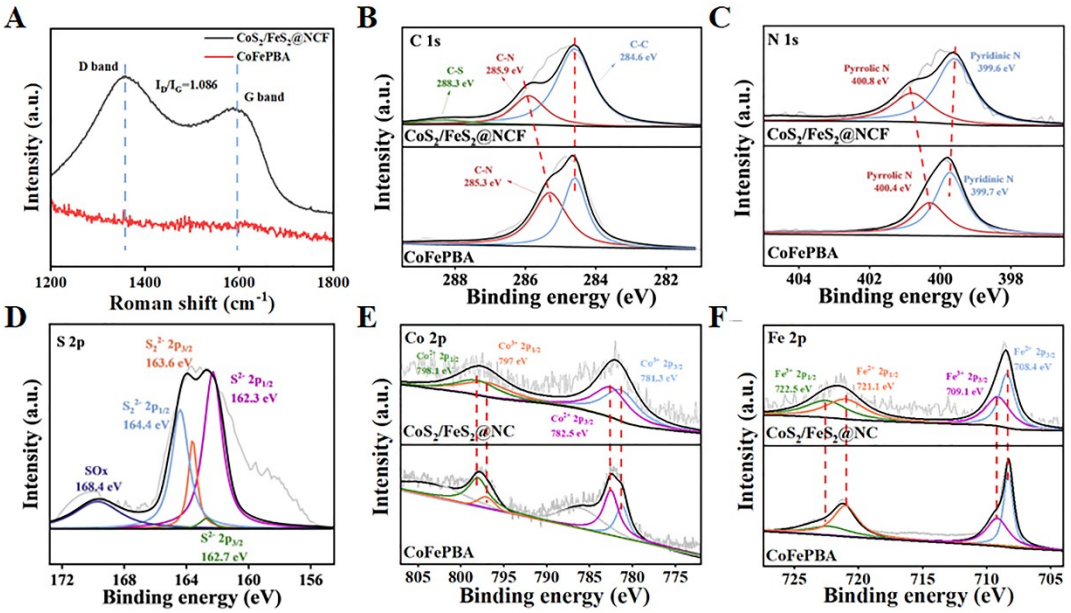

Fig. S2 (A) Raman spectrum of CoS_2/FeS_2@NCF and CoFePBA; XPS scan spectra of CoS_2/FeS_2@NCF: (B) C 1s, (C) N 1s, (D) S 2p, (E) Co 2p, and (F) Fe 2p

3.2. Catalytic and Antibacterial Mechanism of POD-like Activity

To optimize the practical application performance of the CoS_2/FeS_2@NCF nanocube, the effects of pH value, substrate concentration, catalyst dosage, and reaction time on its POD-like activity were systematically investigated (Fig. S3). Experimental results show that: the material exhibited the strongest catalytic activity at 652 nm in a pH=4.0 buffer system (Fig. S3A); the catalytic reaction reached a saturation state when the TMB concentration increased to 0.7 mM (Fig. S3B); the activity peaked at a nanozyme dosage of 70 μg/mL (Fig. S3C); kinetic analysis of the reaction revealed that the absorbance of the system rapidly reached a stable value within 3 minutes (Fig. S3D). In summary, the optimal reaction conditions were determined as pH=4.0, a TMB concentration of 0.7 mM, a catalyst concentration of 70 μg/mL, and a reaction time of 3 minutes, representing the most favorable parameter combination for the reaction.

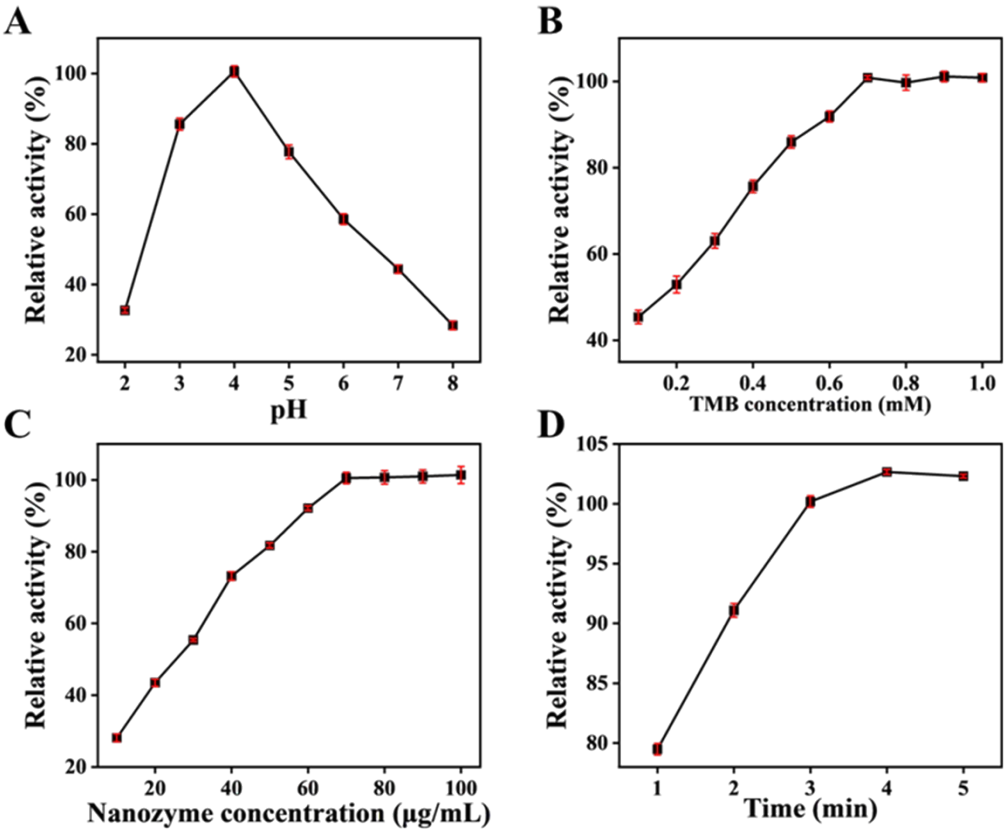

Fig. S3 The optimization of reaction conditions (A) pH, (B) TMB concentration, (C) nanozyme concentration, and (D) reaction time

To analyze the catalytic kinetic characteristics of the CoS_2/FeS_2@NCF CoS_2/FeS_2@NCF nanocube, this study performed kinetic analysis of the TMB- H_2O_2 enzymatic reaction system using the Lineweaver-Burk method (Fig. S4). Through the linear transformation model of the Michaelis-Menten equation, the K_m of the catalyst for TMB and H_2O_2 were calculated to be 0.034 mM and 0.104 mM, respectively, with maximum reaction rates (V_{max}) of 11.058 mmol/s and 11.455 mmol/s, respectively. Compared to the precursor CoFePBA, which exhibited K_m of 0.28 mM for H_2O_2 and 0.32 mM for TMB,[14] the CoS_2/FeS_2@NCF composite demonstrates a synergistic enhancement in these key kinetic parameters. This effect confirms a significantly improved POD-like activity in CoS_2/FeS_2@NCF, driven by both strong substrate binding affinity and high catalytic turnover, collectively leading to a remarkable increase in reaction rate. The lower K_m values indicate high substrate affinity, enabling efficient reaction initiation at low concentrations, while the higher V_{max} demonstrates

rapid substrate conversion under saturation, together reflecting superior catalytic efficiency.[15]

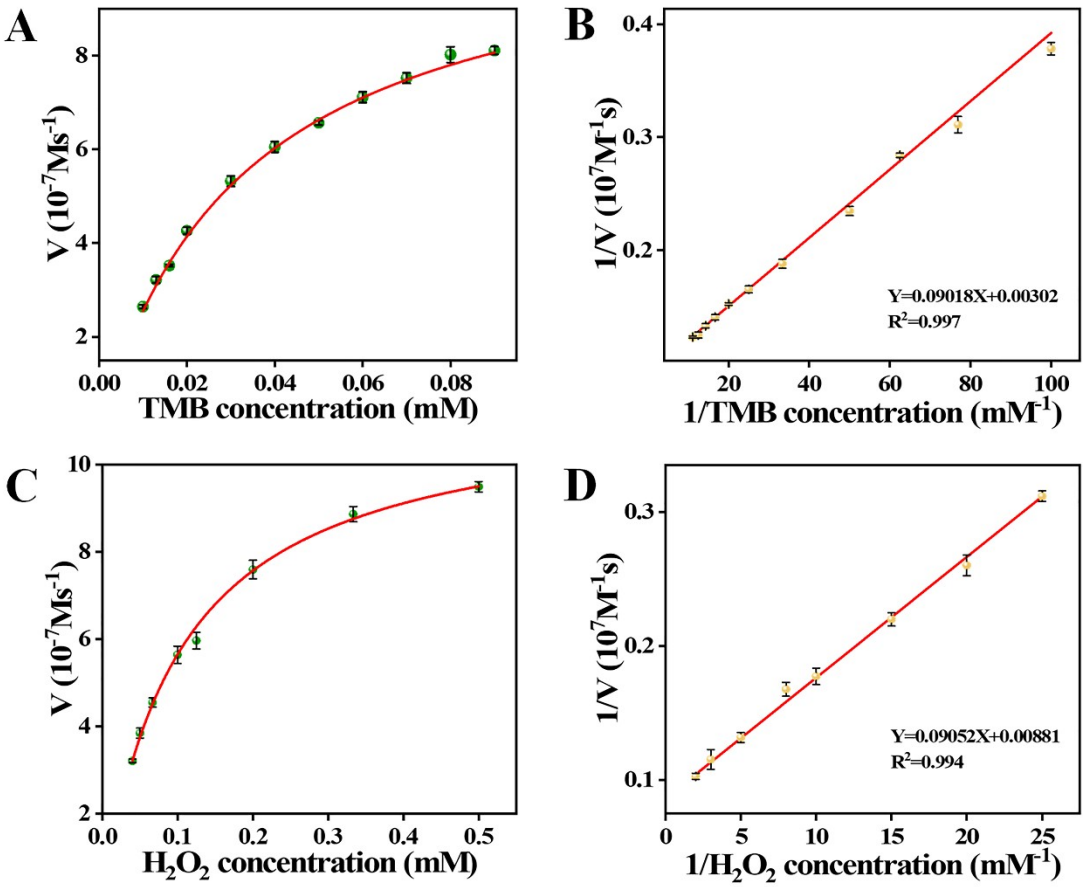

Fig. S4 Enzymatic kinetics analysis of the CoS_2/FeS_2@NCF (A) The concentration of TMB was 1 mM and the H_2O_2 concentration was varied, (C) The concentration of H_2O_2 was 1 mM and the TMB concentration was varied. Lineweaver-Burk plots of CoS_2/FeS_2@NCF (B) TMB as substrate, (D) H_2O_2 as substrate

3.3. In Vitro Antibacterial Activities of CoFePBA and CoS_2/FeS_2@NCF

As shown in Fig. S5, the antibacterial activity of the CoFePBA precursor becomes apparent only at relatively high concentrations (750 μg/mL), achieving over 90% inhibition at 1500 μg/mL. In contrast, this value is much higher than the optimal antibacterial concentration of CoS_2/FeS_2@NCF (300 μg/mL).

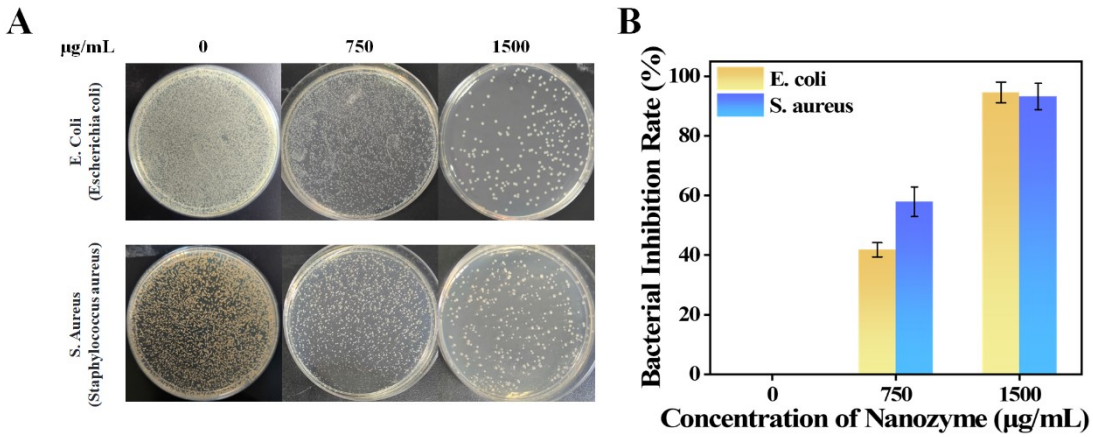

Fig. S5 Standard agar plates treated with CoFePBA: (A) Photograph of E. coli and S. aureus; Bacterial inhibition rate of (B) E. coli and S. aureus.

To elucidate the primary antibacterial mechanism, a control experiment was conducted using CoS_2/FeS_2@NCF without H_2O_2. The absence of significant bacterial inhibition (Fig. S6) unequivocally demonstrates that the lethal effect is catalytically driven by •OH generation, rather than stemming from physical damage or intrinsic material toxicity. The enhanced hydrophilicity thus acts as a critical potentiating factor by improving interfacial contact and mass transfer, thereby maximizing the efficiency of the catalysis-based antibacterial process.

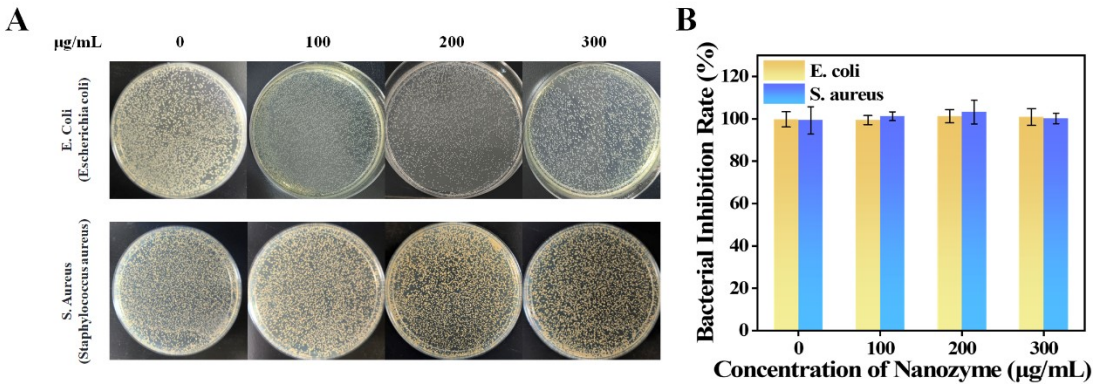

Fig. S6 Standard agar plates treated with CoS_2/FeS_2@NCF without H_2O_2: (A) Photograph of E. coli and S. aureus; Relative survival rate of (B) E. coli and S. aureus.

References

1 L.-C. Wang, P.-Y. Chiou, Y.-P. Hsu, C.-L. Lee, C.-H. Hung, Y.-H. Wu, W.-J. Wang, G.-L. Hsieh, Y.-C. Chen, L.-C. Chang, W.-P. Su, D. Manoharan, M.-C. Liao, S. Thangudu, W.-P. Li, C.-H. Su, H.-K. Tian and C.-S. Yeh, *Nat Commun*, 2023, **14**, 4709.

2 Y. Feng, F. Chen, J. M. Rosenholm, L. Liu and H. Zhang, *Mater. Futures*, 2022, **1**, 023502.

3 L. Li, D. Wang, L. Ren, T. Wang, X. Tan, F. Cui, T. Li and J. Li, *International Journal of Biological Macromolecules*, 2024, **258**, 129098.

4 Y. Ru, D. G. Evans, H. Zhu and W. Yang, *RSC Adv.*, 2013, **4**, 71–75.

5 J. Xu, M. Wang, N. P. Wickramaratne, M. Jaroniec, S. Dou and L. Dai, *Advanced Materials*, 2015, **27**, 2042–2048.

6 R. Zang, P. Li, X. Guo, Z. Man, S. Zhang, C. Wang and G. Wang, *J. Mater. Chem. A*, 2019, **7**, 14051–14059.

7 J.-H. Kim, J. W. Bang and S. Seo, *Science of Advanced Materials*, 2016, **8**, 47–51.

8 N. R. Chodankar, S.-H. Ji, Y.-K. Han and D.-H. Kim, *Nano-Micro Lett.*, 2019, **12**, 1.

9 S.-X. Pan, T.-Z. Xie, T.-F. Xiao and J.-H. Xie, *RSC Adv.*, 2020, **10**, 44470–44480.

10 I. Montenegro, E. Sánchez, E. Werner, P. Godoy, Y. Olguín, N. Caro, N. Ehrenfeld and A. Madrid, *BMC Chemistry*, 2019, **13**, 1.

11 L. Sun, X. Liang, H. Liu, H. Cao, X. Liu, Y. Jin, X. Li, S. Chen and X. Wu, *Journal of Hazardous Materials*, 2023, **452**, 131319.

12 A. Hanan, D. Shu, U. Aftab, D. Cao, A. J. Laghari, M. Y. Solangi, M. I. Abro, A. Nafady, B. Vigolo, A. Tahira and Z. H. Ibupoto, *International Journal of Hydrogen Energy*, 2022, **47**, 33919–33937.

13 K. Li, Y. Zhang, G. Qu and C. Xu, *Separation and Purification Technology*, 2024, **344**, 127223.

14 F. Shi, H. Zhu, G. Li, M. Peng, Y. Cao, Y. Xia, C. Ren, J. Li and Z. Yang, *Anal. Chem.*, 2025, **97**, 7128–7137.

15 Y. Lin, T. Wang, Y. Liu, L. Pu, M. Jia, X. Zhou, L. Ding, W. Zhu and K. Wang, *Analytica Chimica Acta*, 2025, **1353**, 343976.